Robust Control for Active Debris Removal of a Large Flexible Space Structure

Singh, Sunayna; Mooij, Erwin

DOI
10.2514/6.2020-2077

Publication date
2020

Document Version
Final published version

Published in
AIAA Scitech 2020 Forum

AIAA SciTech Forum
6-10 January 2020, Orlando, FL
AIAA Scitech 2020 Forum

10.2514/6.2020-2077

Robust Control For Active Debris Removal of a Large Flexible Space Structure

Sunayna Singh*and Erwin Mooij†
Delft University of Technology, Faculty of Aerospace Engineering,
Kluyverweg 1, 2629 HS Delft, The Netherlands

This paper examines the dynamics and control involved in the active removal of a large space debris - Envisat. In the light of European Space Agaency's e.deorbit mission, the current mission scenario consists of a chaser satellite, synchronising, capturing and detumbling the large uncooperative debris. A unique multibody approach based on floating frames is used to model the Flexible Multibody Dynamics. The controllability characteristics of a linear PD controller and an Incremental Nonlinear Dynamic Inversion controller are also studied. From previous research, it was found that in the docked configuration, the control of the system could not be achieved due to the complex elastic dynamics originating from the large solar panel of Envisat (14.2 m). This paper focuses on achieving robust control of this phase through advanced design choices in both structural and control aspects. It was found that the inclusion of structural damping and reduction of control limits, lead to a major improvement in controllability of the system. A basic digital notch filter did not prove effective for more robust control. This is because only a high order filter could account for the low frequency vibrations. Further, it also required retuning of the controller within the flexible model. These two aspects proved to be beyond computational capabilities. A simple control strategy of introducing a dead-band in control loop improved the control response considerably by allowing the disturbing frequencies to dampen out.

I. Introduction

For any spacecraft in the vicinity of Earth or in the inner Solar System, solar power is the main source of energy, making the solar panel a critical design aspect. Larger power requirements lead to larger solar arrays, thereby resulting in Large Flexible Space Structures (LFSS). Some well known examples of such structures include the International Space Station (ISS) and ESA's successful mission to comet 67P/Churyumev-Gerasimenko, Rosetta. Being a manned space station, the ISS performs multiple Rendezvous and Docking (RVD) operations a year for supplies and scientific research. Additionally, it also performs numerous attitude corrective and collision avoidance manoeuvres to maintain its altitude and to avoid any imminent threat from space debris in the crowded Low Earth Orbit (LEO). With four sets of large solar arrays spanning 2500 m^2, performing these operations may introduce complex flexible dynamics, which affect the overall spacecraft attitude. If left uncontrolled, the vibrations induced in the flexible elements can lead to total loss of control of the spacecraft. Therefore, the ISS holds a robust Attitude and Orbit Control System (AOCS) to ensure efficient functioning of the space station. Similarly, Rosetta, the first deep space mission to be entirely powered by solar energy, experienced vibrations in its attitude due to the interaction of its large appendages (two 14 m long solar array wings) with the drag originating from the comet. Evidently, the challenge associated with the dynamics and control of LFSS is frequent in the space industry. Some other applications include on-orbit assembly of space structures, deployment and retrieval of solar appendages, slew manoeuvres and precision pointing in the presence of external perturbations. A more contemporary application of this field is the active debris removal of large space structures. This application will be the

*Research Engineer, German Aerospace Center (DLR), Bremen, Germany, Sunayna.Singh@dlr.de
†Assistant Professor, section Astrodynamics and Space Missions, e.mooij@tudelft.nl, Associate Fellow AIAA.

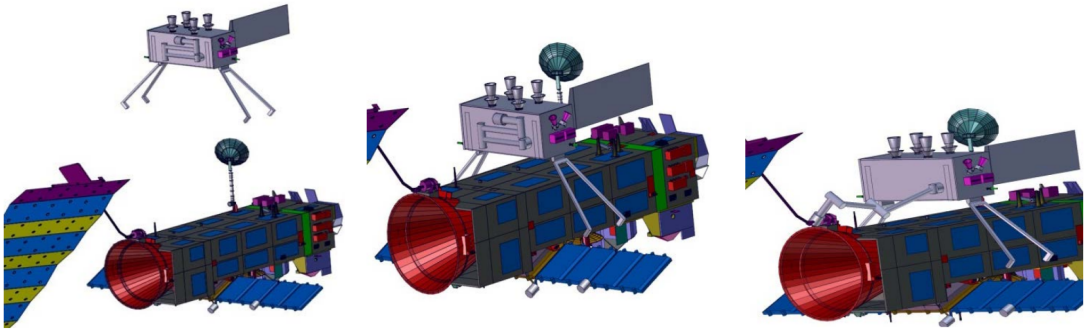

(a) Deploy the tentacles (b) Approach Envisat (c) Deploy Envisat and grab solar panel boom

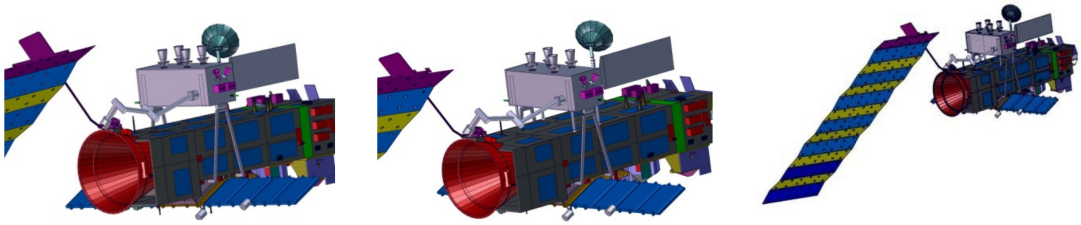

(d) Close the tentacle arms (e) Deploy the pushing rods (f) Stabilise stack for deorbiting

Figure 1. Phases of e.deorbit mission showing interaction of chaser with Envisat (Credits: ESA)

main focus of this paper and will be discussed in further detail.

Since the onset of Space Age, the number of satellites launched every year has been increasing progressively. Unfortunately, most objects launched into space are still orbiting the Earth even though only a small fraction of them is operational. These inactive objects or space debris, pose a major threat to the current and future of space exploration. If the growth of the debris population, especially in LEO is not contained, the debris may collide with each other and with the active satellites, leading to a cascade of collisions and rendering the orbit unusable. To avoid such a catastrophic scenario, it is not sufficient to just avoid collisions with the active satellites, and there is a need to remove any large debris that can contribute to the rise in debris population. ESA's e.deorbit mission aims at developing new technologies for actively removing such large objects to mitigate the current space debris scenario and bring increased attention to environmental impacts of its activities in space. One of the promising concepts includes a chaser with tentacles and an optional robotic arm to capture the debris and is the basis of this research. The main target debris for the mission is ESA's largest Earth observation satellite, Envisat. The eight tonne satellite with a 14.2 m long solar array lost contact on April, 2012, after 10 years of successful operation. The debris is tumbling uncontrollably and poses the highest collision risk of all ESA owned satellites in the densely populated altitude of 600-800 km near polar orbit. Since the debris can also be categorised as a LFSS, it proves to be an ideal case study for this research.

The different phases as defined by e.deorbit for active removal of Envisat using a chaser with tentacles can be visualised using Fig. 1. However, for the purpose of this research, the process is condensed to three main phases: the synchronisation phase, semi-connected phase and the connected phase. In the synchronisation phase, the two bodies are unconnected and the chaser synchronises with the tumbling motion of the target. In the semi-connected phase, the chaser is connected to the target but a rigid attachment is not achieved. Lastly, in the connected phase, the chaser is rigidly connected to the target debris and can now stabilise its motion. The presence of large flexible appendages and multiple bodies stacked into one configuration, characterises a nonlinear flexible multibody problem.

The goal of this research to study the interaction between rigid body and flexible body dynamics associated with active debris removal using a chaser spacecraft, and its effect on controller performance using a novel multibody approach. The new and unique multibody approach based on floating frames,[1] enables easy modelling of constraints and provides a good balance between accuracy and computation time. Further, the

performance of a linear PD controller is compared against a nonlinear controller - Incremental Nonlinear Dynamic Inversion (INDI). From previous research presented in Ref. 2, it was found that for the synchronisation phase, both controllers successfully synchronise the chaser with the target debris tumbling at the rate of 3.5 °/s about all axes. The chaser panel showed a dominantly rigid behaviour and no flexible vibrations were observed. However, during the connected phase, the large appendage (14.2 m) in the stacked configuration introduces complex dynamics, which could not be stabilised by applied controllers. The semi-connected phase was not modelled and will be covered in future research. The current paper aims to continue this study, by pursuing a robust control over the connected phase of the mission, through mindful design choices in both structural and control aspects.

In this paper, the flexible multibody model is discussed in Sec. II. This includes a summarised derivation of the equations of motion (EOM) for the multibody system using the new modelling method. Also, the physical or structural model of the system, which is adapted to fit the new multibody method is discussed. Next, in Sec. III, the basic control theory for the controllers used in the study is discussed. The architecture of the simulator and specifications for simulations are also presented here. The section is concluded with a brief outlook of the results obtained from previous research. Section IV consists of the important design modifications made for improved control of the connected phase. The results from the new simulations are presented in Sec. V. Lastly, the outcome of this paper is concluded in Sec. VI and some recommendations are made for future research.

II. Flexible Multibody Model

Most spacecraft today can be defined as a multibody system consisting of rigid and flexible elements. For a quick judgement of motion in a multibody system, often it is acceptable that the elements of the system are considered rigid. However, when high accuracy is required (for instance, in case of precision control), the flexibility cannot be ignored. Therefore, the complete dynamics including the flexibility must be modelled for the current application. Often defining very complex systems with multiple flexible elements entails large computation times for an accurate model, with an added complication of constraint modelling. While there are many possible ways to define the FMD, from the previous research[2] it was found that the floating frame provides a combined advantage of accuracy and low computation time as compared to other common multibody formulations, like inertial frame and corotational frame formulations. The new method, which is a modification to the standard floating frame formulation further escalates the advantage by enabling easy constraint handling and possibility of model reduction. A brief methodology of this modelling technique will be presented in Sec. II.A. A more detailed mathematical model can be found in Ref. 2.

To study the dynamics of the system, the system configuration should be structurally defined in a way that is compatible with the chosen FMD technique. Further, the discretisation, material properties and mass properties should also be selected such that the physical properties of the satellite are closely represented. These aspects of the model will be discussed in Sec. II.B.

A. Flexible Multibody Dynamics

The vibrations induced due to flexibility act like perturbations to the rigid body motion, which is the dominating component. This means it is possible to define the motion of the complete system by superimposing small nonlinear elastic deformations on the rigid body motion, also known as mean rigid body motion. In the floating frame, this motion is typically represented using a frame attached to the body, which moves along with the body. It is commonly placed at joints between two bodies, known as interaction points (however, it can be placed anywhere on the body). The elastic perturbations can be estimated using the mode shapes and eigenfrequencies, which are either determined numerically or experimentally. The classical formulation despite providing good accuracy without compromising on the computation time, poses a challenge in terms of constraint handling for very complex structures. It requires the use of Lagrange multipliers, which act like added EOM to the system. This makes the method relatively difficult to model for complex structures and also, adds to the computation time (due to the extra number of unknowns in the EOM). The new method, which uses absolute interface coordinates to define the FMD in the floating frame formulation, eliminates this disadvantage, resulting in an efficient formulation.

The term absolute coordinates here refers to the generalised coordinates defined with respect to the global inertial frame. Figure 2 shows a chain of three bodies connected at interface points P_j and P_k, with

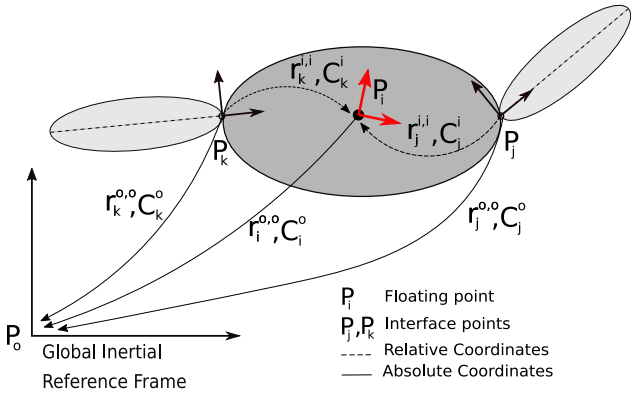

Figure 2. Relative and absolute representation of interface points, P_j and P_k

the floating frame located at P_i. The relative position or local position of the interface points is defined with respect to the floating frame using generalised coordinates, $\boldsymbol{q}^{\boldsymbol{i,i}}_{\boldsymbol{j}}$ and $\boldsymbol{q}^{\boldsymbol{i,i}}_{\boldsymbol{k}}$. To define the absolute position or the global position, the floating frame is first defined with respect to the inertial frame using $\{\boldsymbol{r}^{\boldsymbol{o,o}}_{\boldsymbol{i}}, \boldsymbol{C}^{\boldsymbol{o}}_{\boldsymbol{i}}\}$, which define the position vector and rotation matrix respectively. The global position of the interface points can now be derived by performing a simple transformation and eliminating the floating frame. Now the position of P_j and P_k can be defined using $\{\boldsymbol{r}^{\boldsymbol{o,o}}_{\boldsymbol{j}}, \boldsymbol{C}^{\boldsymbol{o}}_{\boldsymbol{j}}\}$ and $\{\boldsymbol{r}^{\boldsymbol{o,o}}_{\boldsymbol{k}}, \boldsymbol{C}^{\boldsymbol{o}}_{\boldsymbol{k}}\}$ respectively. This process can be repeated for N number of interface points.

Applying these transformations, the final velocity terms (derived in detail in Ref. 1) can be written as follows:

$$\begin{pmatrix} \dot{\boldsymbol{q}}^{\boldsymbol{o,o}}_{\boldsymbol{i}} \\ \dot{\boldsymbol{q}}^{\boldsymbol{i,i}} \end{pmatrix} = \boldsymbol{A}\dot{\boldsymbol{q}}^{\boldsymbol{o,o}}, \qquad \text{where} \qquad \boldsymbol{A} = \begin{bmatrix} [\boldsymbol{C}^{\boldsymbol{o}}_{\boldsymbol{i}}][\boldsymbol{Z}^{\boldsymbol{i}}][\bar{\boldsymbol{C}}^{\boldsymbol{i}}_{\boldsymbol{o}}] \\ [\boldsymbol{T}^{\boldsymbol{i}}][\bar{\boldsymbol{C}}^{\boldsymbol{i}}_{\boldsymbol{o}}] \end{bmatrix} \tag{1}$$

where $\dot{\boldsymbol{q}}^{\boldsymbol{i,i}}$ represents a column matrix containing the local velocities relative to the floating frame representing the elastic deformation in the body. Therefore, Eq. (1) allows the successful formulation of the dynamic equations of floating frame completely in terms of inertial coordinates. The matrices $[\boldsymbol{Z}^{\boldsymbol{i}}]$ and $[\boldsymbol{T}^{\boldsymbol{i}}]$ are the transformation matrices used to transform the rigid body motion and the local elastic motion respectively. A detailed mathematical description of these matrices can be found in Ref. 3. Note that the elastic modes considered in this formulation are the first few dominating frequencies derived using Craig-Bampton reduction (CB).[4] This reduction methods allows reduction of the overall equation of motion, including the mass and stiffness matrices, without loss in accuracy. The final generalised equation of motion is of the form:

$$\boldsymbol{M}\ddot{\boldsymbol{q}} + \boldsymbol{C}\dot{\boldsymbol{q}} + \boldsymbol{K}\boldsymbol{q} = \boldsymbol{F} \tag{2}$$

Here, the $\boldsymbol{M}$ and $\boldsymbol{K}$ denote the global mass and stiffness matrices, $\boldsymbol{q}$ are the generalised coordinates of the floating frame and local frames of the system, $\boldsymbol{C}\dot{\boldsymbol{q}}$ includes the quadratic velocity inertia forces due to terms like damping, centrifugal and Coriolis forces, and lastly, $\boldsymbol{F}$ includes the externally applied forces and moments like gravity gradient, control torques and so on.

To arrive at the final EOM, some simplifying assumptions are made,[5]

1. The mass matrices are expressed in the undeformed configuration of the component (for the acceleration term).

2. The mass matrix is lumped (for the velocity term).

3. Each body is defined by one element at the interface points, which guarantees that the interface points chosen for this formulation and the floating frame formulation are the same (for velocity term).

Additionally, test cases simulated in Ref. 1 prove that neglecting the quadratic inertia terms, do not have a significant impact on the simulation accuracy for small deformation cases. Therefore, for the current simulation, these forces will not be considered. A more detailed derivation of these assumptions can be found in Ref. 5. Using the above stated process, the EOM can be derived to analyse the dynamics of the multibody system. The software based on the formulation was verified and validated using law of conservation

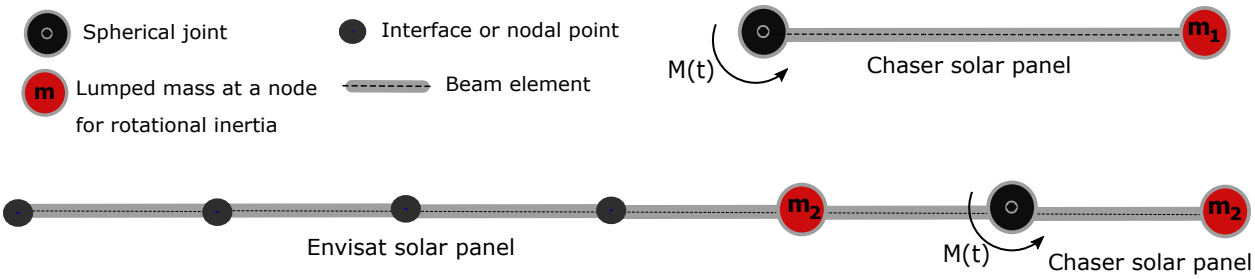

Figure 3. Simplified representation of the structural model for synchronisation (top) and connected (bottom) phases[2]

of energy for some basic mechanical systems, like a slider-crank system, and a beam constrained by spherical joint on one end as shown in Ref. 2. It was concluded that the energy remained conserved for both systems and the formulation is modelled correctly.

B. Structural Model

The structural model of the system can be mainly defined by three aspects:

1. *System Configuration:* To model the vibrational behaviour of the satellite, it is imperative that the mass and inertia properties are captured in the structural model. Since the current paper only aims to improve the control of complex dynamics associated with the connected phase, only the properties of the stacked configuration are required. The stacked configuration consists of the two docked satellites, rigidly attached at the hub, tumbling with the angular velocity of the target debris. The system can be looked at one large rigid hub with two asymmetric flexible appendages. The smaller solar panel from the chaser has dimensions 2.9×1.1×0.05 m and weighs 25 kg. The larger solar panel from Envisat is 14.2 m long and 5 m wide, and weighs 338 kg. The total mass of stacked system is 9308 kg (sum of mass of the participating spacecraft) and the total mass inertia about the principle axes is given by:[2]

$$\boldsymbol{J_{stack}} = \begin{bmatrix} 130521 & 0 & 0 \\ 0 & 27282 & 0 \\ 0 & 0 & 134251 \end{bmatrix} \text{kg m}^2 \tag{3}$$

   While modelling the multibody system, these mass and inertia properties will be maintained.

2. *Modelling of flexible elements:* Since the configuration in the connected phase is asymmetric, especially due to the flexible elements of the system, it is advantageous to model them as beams. This is because the deformation of any material point on these elements can be easily defined with respect to the local frame using established shape functions. From analysis and sensitivity studies shown in Ref. 2, a Young's modulus of 5.8×10^{10} N/m^2 for a 1 m long beam and a Poisson's ratio of 0.3 is chosen. The beam element length for the solar panels is chosen to be 2.9 m. This means that the chaser solar panel could be modelled with one beam element, while the Envisat solar panel would be modelled with five beam elements (14.2 m long). Lastly, while applying boundary conditions, orbital or translational motion of the stack is not considered. Therefore, the centre of mass of the system, where the control moment is applied is constrained using a spherical joint as shown in Fig. 3. This allows the study of dynamics and control associated with only the rotational behaviour of the system.

3. *Modelling of rigid elements:* A dominant characteristic of a rigid body, is its rotational or mass inertia, which is a measure of its resistance to change in orientation. According to Ref. 6, it is possible to add rotational inertia to a flexible system using lumped (point) masses. Figure 3 (bottom) shows lumped masses added to the nodes between each beam element to account for the large inertia of the stacked system. The inertia is translated to these nodes using Steiner's parallel axis theorem. Note that the lumped masses are added only after the Craig-Bampton reduction is performed. This ensures that the lumped masses do not affect the natural frequency of vibration of the flexible elements.

Once the structural dynamics has been established, the next step is to discuss the basics of the controllers used in the research.

III. Control System Design

The control of a massive tumbling body with large, flexible appendages can be challenging, as discrete application of control can lead to oscillations in the solar panels. A system with such complex dynamics may not be successfully controlled with commonly used PD controller. A more robust option to control such uncertain nonlinear dynamics is to choose a controller based on the dynamics of the system itself. The Nonlinear Dynamic Inversion (NDI) controller enables multivariable control and avoids gain-scheduling by directly incorporating the nonlinear dynamics in the control law. However, it can be sensitive to model mismatched and measurement errors, which may result in instability.[7] A modified version of NDI known as INDI reduces the effect of these mismatches and will be used in this research.

Since only the rigid body motion can be controlled using the applied control moment at the COM of the system, the guidance for the control system must be based on the rigid body dynamics. The EOMs used for the guidance are briefly discussed in Sec. III.A. Then, the basics of the control theory are presented in Sec. III.B. Lastly, the architecture of the simulator developed for the analysis of the dynamics and control characteristics of the system will be presented in Sec. III.C.

A. Guidance

As stated before, it is assumed that the rotational motion is decoupled from the translational motion, *i.e.,* the orbital position is frozen. Since the target is rotating with an angular rate of about 3.5°/s, a standard formulation with Euler angles is not possible, due to the presence of singularity in the equations. The common next step to solve this problem would be to use the four-element quaternion representation. However, it was found that the N matrix, that represents the rigid body kinematics in the INDI controller degenerates once the attitude exceeds ±180° of rotation (refer to Sec. III.B). Therefore, an alternative approach was used to solve the problem. By observing the angular rates of a body about an axis, it is possible to derive the evolution of attitude about the same axis by simple integration. This virtually represents the Euler angles without the singularity, and will be referred to as *pseudo Euler angles* for the rest of the research. This representation is applicable only because the orbital motion of the system is not considered, and the *pseudo Euler angles* are sufficient to represent orientation. In future research, a more complicated Modified Rodrigues Parameters must be used for a singularity free representation. The kinematics of the rigid body system can be simply defined using the angular velocity. This gives:

$$\dot{\boldsymbol{\Theta}} = \begin{pmatrix} \dot{\phi} \\ \dot{\theta} \\ \dot{\psi} \end{pmatrix} = \begin{pmatrix} \omega_1 \\ \omega_2 \\ \omega_3 \end{pmatrix} \tag{4}$$

The dynamic EOM for pseudo Euler angles can be found using the Euler's dynamic equations of motion, given by:

$$\boldsymbol{J\dot{\omega} + \Omega J\omega = M_c} \tag{5}$$

where $\boldsymbol{J}$ is the inertia matrix, $\boldsymbol{M_c}$ indicates the control torque and $\boldsymbol{\Omega}$ is the skew-symmetric matrix given by:

$$\boldsymbol{\Omega} = \begin{bmatrix} 0 & -\omega_3 & \omega_2 \\ \omega_3 & 0 & -\omega_1 \\ -\omega_2 & \omega_1 & 0 \end{bmatrix} \tag{6}$$

Equations (4) and (5) together define the guidance state, which is then used to compute the error against the state vector from the plant (the flexible system).

B. Controller Design

A linear PD controller is still among the most widely used controllers for attitude control. These controllers are mostly used for problems where the steady state error is not zero. The control moment for this controller is defined using:

$$\boldsymbol{M_c = -(K_p e + K_d \dot{e})} \tag{7}$$

where $\boldsymbol{K_p}$ and $\boldsymbol{K_d}$ are proportional and derivative gains respectively. $\boldsymbol{e}$ and $\boldsymbol{\dot{e}}$ are the error in state and the state derivative respectively. The error state $\boldsymbol{e}$ can be computed as the difference with the commanded

attitude. Since the commanded attitude rate is zero, $\dot{\boldsymbol{e}}$ depends only on the actual angular rate.

As stated before, the INDI controller is an enhanced modification of the NDI controller. In this controller, the final dynamics case is approximated by a first order Taylor series. With the notation "0" indicating the nominal case, the dynamics can be approximated by:

$$\dot{\boldsymbol{\omega}} \approx \dot{\boldsymbol{\omega}}_{\mathbf{0}} + \frac{\partial \dot{\boldsymbol{\omega}}}{\partial \boldsymbol{\omega}}(\boldsymbol{\omega} - \boldsymbol{\omega}_{\mathbf{0}}) + \frac{\partial \dot{\boldsymbol{\omega}}}{\partial \boldsymbol{u}}(\boldsymbol{u} - \boldsymbol{u}_{\mathbf{0}}) \tag{8}$$

where the partial derivatives are evaluated at $\boldsymbol{\omega} = \boldsymbol{\omega}_{\mathbf{0}}, \boldsymbol{u} = \boldsymbol{u}_{\mathbf{0}}$. The first term of the equation is the angular acceleration obtained from onboard sensors. For high sampling rates, when the difference between new and current angular acceleration becomes small, the equation can be further reduced. The partial derivative with respect to the state, *i.e.*, the second term can be neglected. Therefore, the equation becomes

$$\dot{\boldsymbol{\omega}} \approx \dot{\boldsymbol{\omega}}_{\mathbf{0}} + \frac{\partial \dot{\boldsymbol{\omega}}}{\partial \boldsymbol{u}}(\boldsymbol{u} - \boldsymbol{u}_{\mathbf{0}}) \tag{9}$$

The second partial derivative can be found from the dynamic equation of motion, Eq. (5), which is simply found to be $\frac{\partial \dot{\boldsymbol{\omega}}}{\partial \boldsymbol{u}} = \boldsymbol{J}^{-\mathbf{1}}$. Using the notation $\boldsymbol{\Delta M_c} = \boldsymbol{u} - \boldsymbol{u}_{\mathbf{0}}$ and re-arranging Eq. (9), we get:

$$\boldsymbol{\Delta M_c} = \boldsymbol{J}(\boldsymbol{v} - \dot{\boldsymbol{\omega}}_{\mathbf{0}}) \tag{10}$$

The virtual control term ($\boldsymbol{v}$) is computed using a PD controller with dynamic inversion, which is applied in two loops. This is done to obtain a Time Scale Separation in the inversion of dynamics, which allows quicker control. The outer loop is defined by:

$$\dot{\boldsymbol{x}}_{\mathbf{2}} = \boldsymbol{N}\boldsymbol{u}_{\mathbf{2}} \tag{11}$$

where $\boldsymbol{x}_{\mathbf{2}} = \boldsymbol{\theta}$, $\boldsymbol{u}_{\mathbf{2}} = \boldsymbol{\omega}$ and $\boldsymbol{N}$ is a matrix used for dynamic inversion of the plant given by Eq. (4). It can be defined as the coefficient matrix that establishes the relation between the rate of change of attitude, $\dot{\boldsymbol{\Theta}}$ with the angular rates of the system, $\boldsymbol{\omega}$. From Eq. (4), it can be concluded that $\boldsymbol{N}$ becomes an identity matrix for this formulation.

Going back to the outer loop, the virtual control is defined by the error in attitude (as compared to commanded) and the proportional gain.

$$\boldsymbol{v}_{\mathbf{2}} = -\boldsymbol{K}_{\boldsymbol{p}}\boldsymbol{e} \tag{12}$$

This is used by the outer loop to get the first control vector $\boldsymbol{u}_{\mathbf{2}}$,

$$\boldsymbol{u}_{\mathbf{2}} = \boldsymbol{N}^{-\mathbf{1}}(\boldsymbol{v}_{\mathbf{2}}) \tag{13}$$

This control vector $\boldsymbol{u}_{\mathbf{2}}$, is then fed as a reference to compute the virtual control again in the inner loop, it is given by:

$$\boldsymbol{v} = -\boldsymbol{K}_{\boldsymbol{d}}(\boldsymbol{x}_{\mathbf{1}} - \boldsymbol{u}_{\mathbf{2}}) \tag{14}$$

This can be substituted into Eq. (10) to obtain the change in control effort (ΔM_c) The final control torque is given by:

$$\boldsymbol{M_c} = \boldsymbol{M}_{\boldsymbol{c},\mathbf{0}} + \boldsymbol{\Delta M_c} \tag{15}$$

Having discussed the theory for the two controllers used in this research, the simulator design can now be discussed.

C. Simulator Design

In the previous sections, the theory behind different aspects of the research was presented. The theory can be now combined into the simulator architecture based on the basics of a Guidance, Navigation and Control (GNC) system. Figure A1 in the appendix shows a detailed schematic of the simulator with the plant indicated in blue, guidance in orange and control system in green colour. It is assumed that the actuators and sensors are ideal. The dynamics of the flexible multibody system is included in the plant. The guidance, which includes the commanded state based on rigid body dynamics sends the target state for error computation. By doing this, the flexible vibrations originating the plant are treated as external perturbations to the control system. The error between the states is then fed into the controller, which computes the required control moment for the plant. The plant uses the control input to propagate to the next state and feeds it back

for error computation. The loop continues until the error between the commanded and current state is very small and the system is stabilised. The used integration method is a high-order, variable-coefficient Ordinary Differential Equation solver, with fixed-leading-coefficient implementation, originally part of the NetLib mathematical library.[8] The dynamics is simulated with a step size of 10^{-3} s and the controller is sampled at 100 Hz. A zero-order hold is used to retain the present control moments, until the current time step matches the control frequency.

With this simulator design, controllability characteristics of a chaser spacecraft performing two stages (synchronisation and connected phase) of Active Debris Removal (ADR) with a large uncontrolled target with flexible appendages was analysed in Ref. 2. Since the controller design remains elementary for a very dynamic model, three sets of target states were analysed. The first set was a more challenging case of the target debris tumbling with an angular velocity of 3.5 °/s about all axes. In the second case, an angular velocity of 1.5 °/s about all axes was controlled. And lastly, an angular velocity of 3.5 °/s about Z-axis only, which is the nominal case given by ESA was considered. The results (refer to Ref. 2 for details) for both phases of e.deorbit mission showed that:

1. *Synchronisation*: It was found that synchronisation using full state control (including both attitude and angular rates) did not lead to stability. This is because the relatively high angular rate of 3.5 °/s about all axes cannot be achieved when attitude control is also performed simultaneously. The (very large) attitude error drives the controller to correct it, slowing the rate control down and drives the system away from achieving the rate. The second option of rate control until a certain threshold and then switching to full control allowed successful synchronisation of the chaser with the tumbling target using both controllers. Further, no oscillations were observed in the system response, which indicates that the chaser appendage does not induce any perturbations due to flexibility and has a dominantly rigid behaviour.

2. *Connected*: For the connected phase, three operations associated with detumbling were simulated. This included detumbling only (controlling angular rate only), detumbling with reorientation (controlling the complete state) and reorientation only (controlling the attitude only). Even with multiple control limits (±10 Nm, ±25 Nm, ±50 Nm and ±100 Nm), the system could not be controlled in all the attitude scenarios stated above. This is because the large solar appendage in the target body introduced large vibrations in the system dynamics, which could not be controlled by either of the chosen controllers. Nonetheless, INDI showed better performance than the PD controller, which destabilised quickly.

To understand the complex behaviour of the connected phase, multiple sensitivity studies were performed. These studies can help improve the system design to obtain improved control over the connected phase. Some aspects that can be revised in the design will be discussed in the coming section.

IV. Design Revision

As stated before, the natural frequency of vibration for the flexible appendages are excited by the application of control moments. These vibrations eventually escalate to a level that cannot be controlled by the chosen controllers. Through some mindful selection of structural and controller design aspects, more robust control can be achieved. The vibration of flexible appendages involve continuous exchange of kinetic and potential energy. In the absence of dissipative forces, the elastic energy of the system keeps increasing, and the system can become too dynamic for the controller to stabilise. Therefore, most flexible space structures have a small amount of structural damping in the system to improve the closed loop stability. In Sec. IV.A. a simple yet effective way of including damping is explained.

The external force acting on the dynamics, which is the control moments play a critical role in the response of the system. While some systems demand fast control, in most flexible systems, a slow control facilitates reduced amplitude of vibrations. Further, some other structural properties, like mass and inertia should also be considered in the design of a control system. In Sec. IV.B , these important design parameters, which were previously not considered, will be evaluated and taken into account for the new design.

According to Ref. 9, application of modern control methods in autonomously stabilising flexible vehicles often results in a feedback compensator that is sensitive to the elastic bending modes. Even with precise modelling of the structural behaviour, there may be unforeseen resonances and uncertainties. A possible way of improving robustness in such scenarios is by using simple structural filters like a low-pass filter or a notch filter, which are commonly used in the aerospace industry for feedback control applications. This option will

Table 1. Damping coefficients for flexible elements

	ξ_n	f_{n1} [Hz]	f_{n2} [Hz]	α	β
Envisat	0.02	0.0563	0.3523	0.0156	0.0122
Chaser	0.005	2.4374	15.2344	0.00014	0.0825

be discussed in further detail in Sec. IV.C. Lastly, robustness can also be achieved by using control strategies derived from the system properties. One such control strategy is presented in Sec. IV.D.

A. Structural Damping

According to Ref. 10, undamped flexible structures in space can have responses, which can increase without limits due to exchange between kinetic and potential energy. At this point, addition of damping removes or dissipates energy from the system, preventing it from reaching an uncontrollable state. Therefore, structural damping becomes very important for stability and control of flexible space structures. According to Refs. 11 and 12, a typical space structure has an effective damping ranging between 0.5% to 3%.

When a system is weakly damped and its eigenfrequencies are well-separated, the effect of cross-damping can be neglected.[13] This assumption, proposed by Lord Rayleigh, simplifies a complex multiple degree of freedom (MDOF) system to a collection of single degree of freedom (SDOF) oscillations. Recalling the first statement, for the current configuration and dynamic modelling, both conditions are true. Damping in space structures is very small, and the dynamic modelling is such that the mass and stiffness matrices used in the EOM can be written in the form, $\boldsymbol{\phi_{CB}^T M \phi_{CB}}$ and $\boldsymbol{\phi_{CB}^T K \phi_{CB}}$, where $\boldsymbol{\phi_{CB}}$ denotes the modal mass matrix after CB reduction. This diagonalises the system and decouples the undamped modes. It is now possible to apply proportional damping or Rayleigh damping, which is widely used to model dissipative behaviour in complex structures. Here, the damping matrix, $\boldsymbol{C}$, can be expressed as a linear combination of mass and stiffness matrices:[13]

$$\boldsymbol{C} = \alpha \boldsymbol{M} + \beta \boldsymbol{K} \tag{16}$$

where α is the mass proportional damping coefficient, and β is the stiffness proportional damping coefficient. These terms can then be related to the damping ratio using:

$$\xi_n = \frac{1}{2\omega_n}\alpha + \frac{\omega_n}{2}\beta \tag{17}$$

where ξ_n is the damping factor, and ω_n is the associated natural frequency. For two natural frequencies, the expression can be written as:

$$\begin{pmatrix} \xi_i \\ \xi_j \end{pmatrix} = \frac{1}{2}\begin{bmatrix} \frac{1}{\omega_i} & \omega_i \\ \frac{1}{\omega_j} & \omega_j \end{bmatrix}\begin{pmatrix} \alpha \\ \beta \end{pmatrix} \tag{18}$$

where subscripts i and j are associated with the first two important natural frequencies. Usually, each natural frequency has a different contribution or critical damping ratio. However, assuming both modes have the same critical damping factor, the values of α and β are tabulated in Table 1 for both chaser and Envisat solar panels. Since the chaser solar panel is smaller and susceptible to smaller vibrations, a smaller value of damping factor can be selected. Envisat solar panel would require larger damping but within the range of structural damping in space structures. Therefore, a damping ratio of 0.005 (0.5%) and 0.02 (2%) is selected for the chaser and Envisat solar panel, respectively. Note that the first two natural frequencies to estimate the damping factor are estimated using the natural frequency of a cantilever beam given by:

$$f_n = \frac{K_n}{2\pi}\sqrt{\frac{EI}{\rho A L^4}} \tag{19}$$

Here, $K_n = 3.52$ for the first mode of vibration and $K_n = 22.0$ for the second mode, E is the Young's modulus in N/m^2, ρ is the density in kg/m^3, A is the cross-sectional area in m^2, I is the area moment of inertia in m^4 for a rectangular cross-section. A disadvantage of Rayleigh damping is that it proves to be ineffective when a wide range of frequencies is considered.[13] However, the new dynamic multibody modelling method used in this research considers only reduced modes or important modes. Therefore, Rayleigh damping still performs well for this method. The assumption of proportional damping also reduces the computation time, making it well suited for control applications with longer simulation times.

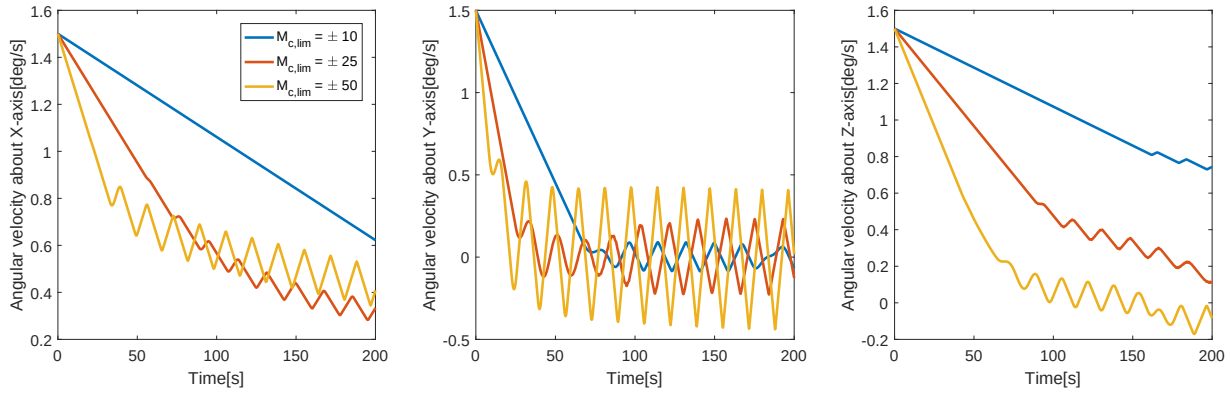

Figure 4. Angular velocity sensitivity to different control moments for detumbling

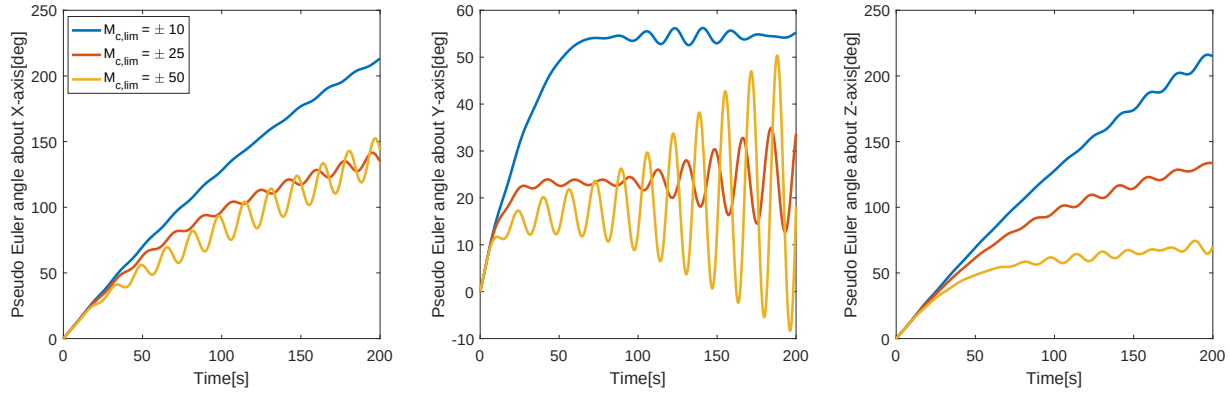

Figure 5. Attitude sensitivity to different control moments for detumbling

B. Control Moments

A sudden change in attitude is caused by control moments, which in turn induces vibrations in the flexible appendages. A larger change in control moment can lead to a larger change in attitude. Figures 4 and 5 show the angular velocity evolution and attitude during the detumbling operation from 1.5°/s about all axes to zero, using three different control limits of ±10 Nm, ±25 Nm and ±50 Nm. From this sensitivity study, it can be observed that the smaller the control limit, the smaller are the induced vibrations. This means that a slower detumbling would improve the controllability of the stacked system. However, if the control limit is too small, the convergence time to attain zero angular velocity will become too large. Therefore, to ensure that the computation time is not too large, the control limit will be set to ±10 Nm.

Another observation that can be made from Fig. 4, is that the amplitude of vibration along Y-axis increases, when the vibrations start appearing along the other axes. This indicates that there is a coupling between the three axes. From Eq. (3) it can be seen that the inertia about X-axis and Z-axis is approximately five times of the inertia about Y-axis. Therefore, the angular velocity about Y-axis converges a lot faster and oscillations start to appear way before the other two axes for the same control limit. These vibrations get amplified when the other two axes start braking. The effect of this can be minimised by ensuring that all axes converge closely and there are smaller accumulated vibrations. This can be achieved by scaling the control limits to the difference in the inertia about the three axis. Again, if the control limit is too small, the convergence time might become too large. Therefore, a control limit of ±10 Nm is set for X-axis and Z-axis, while the control limit for Y-axis is reduced to ±5 Nm.

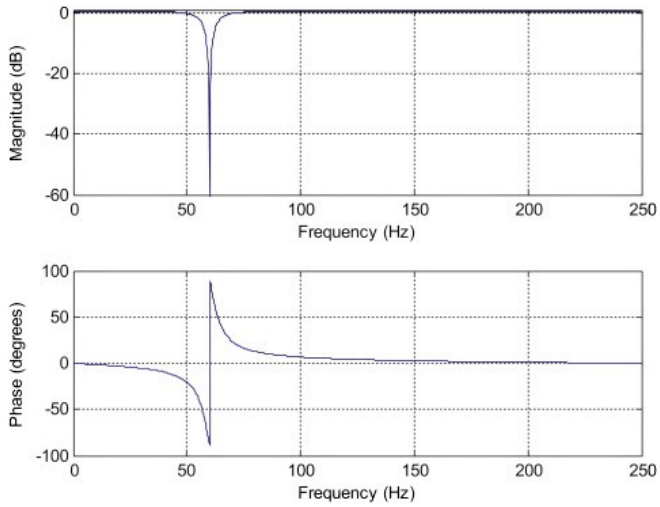

Figure 6. Amplitude and phase behaviour of a notch filter,[14] (ζ=0.15)

C. Bending Filters

Filters are extensively used in control systems to reduce noise and mitigate resonances. Low pass filters are the most commonly used filters for a variety of applications. They are used to eliminate a variety of noise originating from resolution limitations, electro-magnetic interference, intrinsic sources and so on.[15] A special variation of low pass filter, known as a moving average filter, can help provide a smooth output by replacing a sharp data point by average of its neighbouring dataset. The averaging window can be moved over the data with time, to obtain an overall smoother response. However, for it to work effectively, the filter can require a large number of samples depending on the frequency to be filtered. The filter window should contain multiple cycles of the offending frequency, which in the current application can prove to be disadvantageous by adding to the computation time. Especially because the vibrations identified in the previous study shown in Ref. 2 have a period of approximately 17 s, which consists of a large dataset. Therefore, this option will not be considered for this paper.

Notch filters, also known as band-reject or band-stop filters have a more limited application, and are less frequently used compared to low-pass filters. They are used to reject frequencies in a specified range and remove any resonances. They often require tuning as the resonant frequencies change from one system to another. If the offending frequency is known, a digital notch filter can filter the frequency with great accuracy. In this research, since the sensors and actuators are assumed ideal, there is no noise (errors or biases) arising from them. However, from the previous simulations as shown in Ref. 2, the dominating frequency was already identified to be approximately 0.055 Hz. This makes the use of notch filter fitting for this application. A typical notch filter has a second-order transfer function of the form:

$$T(s) = \frac{s^2 + \omega_N^2}{s^2 + 2\zeta\omega_N s + \omega_N^2} \tag{20}$$

where ω_N is the input notch frequency to be filtered in rad/s and ζ is the damping ratio. According to Ref. 15, for a notch filter, the damping ratio is selected to be less than 1. The lower the damping ratio, the sharper is the notch, which is shown in Fig. 6 (top). It also results in a lower phase lag caused below the notch center frequency shown in Fig. 6 (bottom). In practice, the notch filter cannot cancel the disturbing frequency completely (due to round-off errors in digital filters), but still works well enough for most control applications. If more than one frequency requires strong attenuation, multiple notch filters can be used.

D. Control Strategy

From previous study included in Ref. 2, it was found that the vibrations in the system get worse over time due to the control action. A possible control strategy that can be tested for such a scenario is by introducing a control moment dead-band in the presence of structural damping. In other words, once the response about a particular axis has converged sufficiently, the control moments are turned off. This stops the amplitude

from increasing under control action, and subsequently allows the structural damping to damp the vibrations out. The control can then be restarted with lower gains to achieve fine control and minimize vibrations in the structure. While it is also possible to perform the complete simulation with lower control gains to avoid any vibrations at all, the computation and convergence time will become very large. Therefore, the dead-band control strategy provides an option to obtain faster convergence and effective control.

These four design approaches stated above will be applied to the research and the results will be presented in the coming section.

V. Results

This paper aimed to achieve a more robust control over the connected phase associated with active debris removal using a chaser spacecraft. The large asymmetric flexible configuration under control action suffered from large vibrations that could not be controlled by fundamental application of PD and INDI control in the previous research.[2] In this research, three additional design aspects are included to achieve improved control over the tumbling body with complex dynamics. The simulations are now performed with 0.5% damping ratio for the chaser panel and 2% damping ratio for the Envisat solar panel. The control moments are scaled down to $\pm(10,\ 5,\ 10)$ Nm to account for the inertia difference and to minimise the vibrations induced due to control moments. Then, a notch filter will be tested to attenuate any unwanted vibrations in the feedback loop. Lastly, a control strategy based on the system properties will be examined to obtain a smoother response.

An angular velocity of $3.5°/s$ about all axes required large computation time of greater than 2000 s with the reduced moments. And, in the presence of damping, higher computation effort is required. So, this attitude scenario could not be completed with the available computational resources in an acceptable time. Therefore, simulations are made with an initial angular velocity of $1.5°/s$ about all axes, and the results will be analysed using the two controllers (PD and INDI) for all operations in the connected phase: detumbling only, detumbling and reorientation, reorientation only (a detailed description of simulation cases can be found in Ref. 2). The results will be presented in three parts, first without a filter in Sec. V.A and then, with the notch filter in Sec. V.B. In the last part, the dead-band control strategy is tested in Sec. V.C.

A. Without Notch Filter

The results presented in this section, only includes the simulations with the structural damping and the modified control limits. This facilitates the comparison of flexible dynamics observed in the previous research and understand the impact of these design aspects in the absence of any bending filter. Further, the results are also critical to understand the need for such a filter.

A.1. Detumbling Only

Figure 7 shows the detumbling of the stacked configuration with structural damping included. Compared to results obtained without damping (see Fig. 4), the performance has improved considerably. Since the vibrations in angular velocity, which were previously upto $\pm 0.5°/s$ for a control limit of 10 Nm about all axes, have reduced to $\pm 0.1°/s$. The norm of the angular velocity also indicates good convergence. Further, the rather rapid growth in vibration that was observed in the absence of damping has reduced considerably. However, the small vibrations in the system could not be damped out with the current value of damping ratio. Also, the deorbitation manoeuvre being a finite time burn, can last several tens of minutes as suggested in Ref. 16 (even lasting more than a full orbit). During this time, the closed-loop feedback guidance would have sufficient opportunity to correct for any thrust orientation mismatch that may result from the flexible perturbations. Therefore, the vibrations (even though not ideal) can still be considered acceptable for a deorbitation manoeuvre of a certain range of time.

A.2. Detumbling and Reorientation

Figure 8 shows the detumbling and reorientation manoeuvre using the INDI controller. It can be seen that the Y-axis has achieved rigid body convergence, but experiences small perturbations due to the flexibility. The X- and Z-axes require more time for convergence, but are expected to behave similarly.

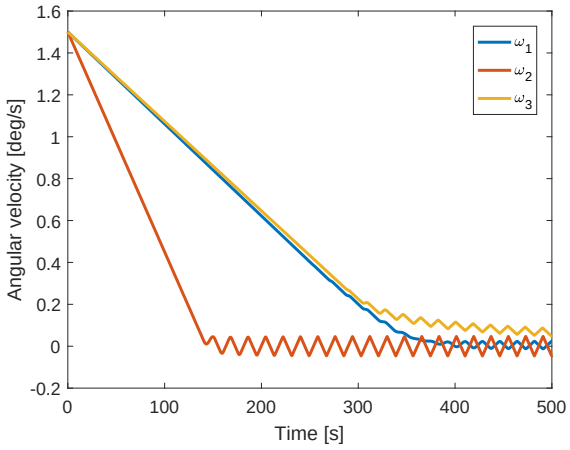

(a) Angular rates

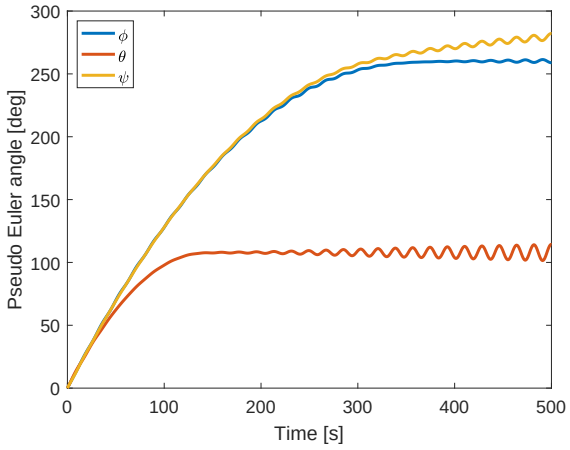

(b) Pseudo Euler angles

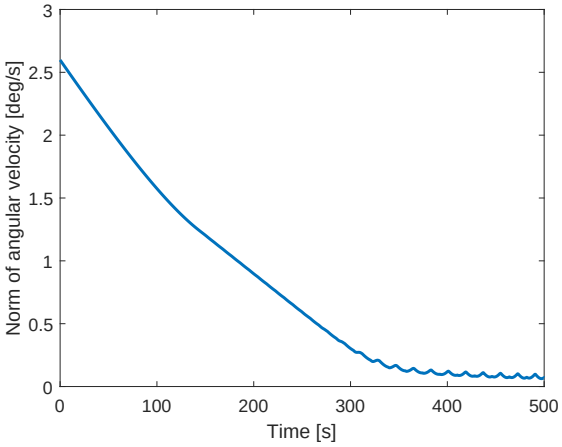

(c) Norm of angular velocity

Figure 7. Flexible multibody control (with damping)- Detumbling only $\mathbf{M}_{c,lim} = \pm$(10, 5, 10) Nm

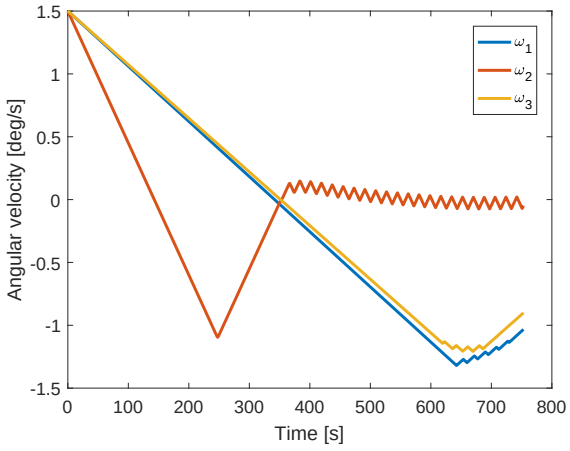

(a) Angular rates

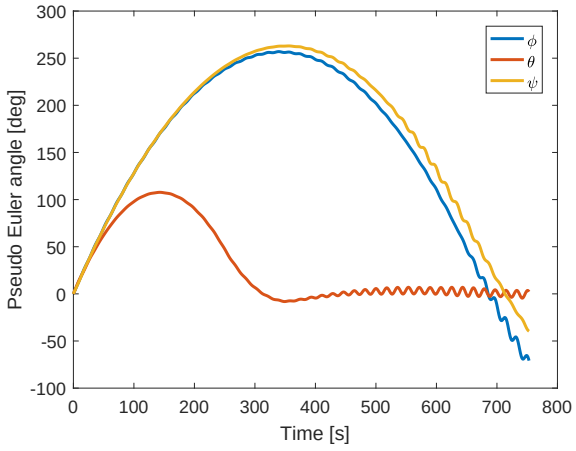

(b) Pseudo Euler angles

Figure 8. Flexible multibody control (with damping)- Detumbling + Reorientation with INDI

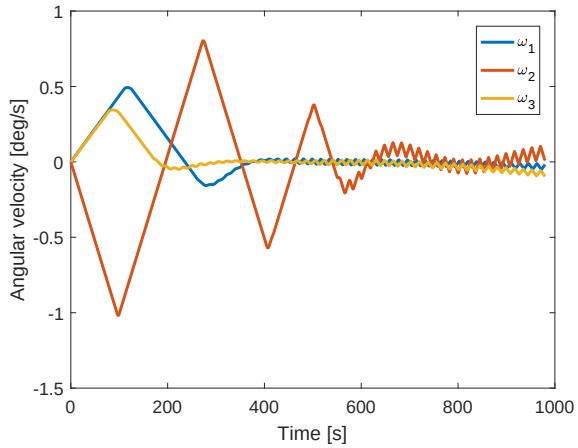

(a) PD angular rates

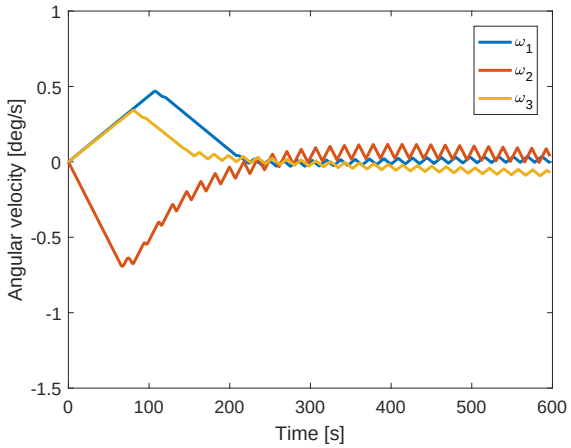

(b) INDI angular rates

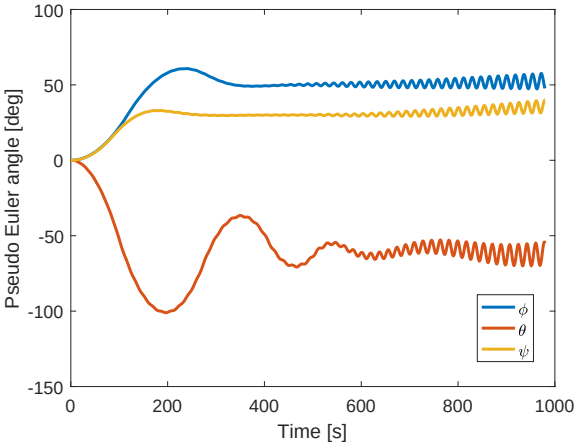

(c) PD pseudo Euler angles

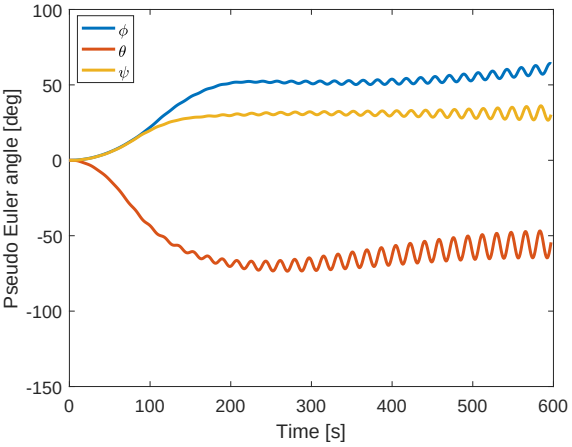

(d) INDI pseudo Euler angles

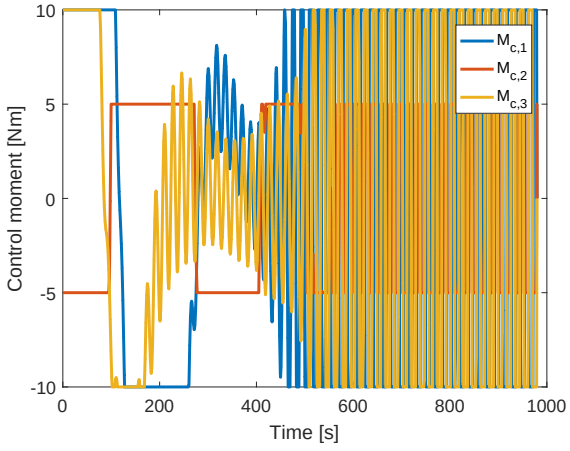

(e) PD control moments

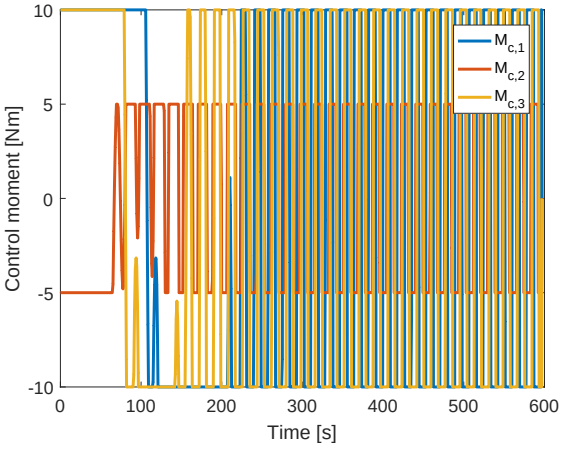

(f) INDI control moments

Figure 9. Flexible multibody control (with damping)- Reorientation only ($\Theta = (50^\circ, -30^\circ, 60^\circ)^T$)

A.3. Reorientation Only

Figure 9 shows the response of the system while performing reorientation manoeuvre for both PD and INDI controllers. INDI controller converges sooner compared to the PD controller. Again, compared to the undamped case, the performance of both the controllers has improved considerably with the vibrations in angular velocity reduced to $\pm 0.1^\circ/s$. The oscillations induced during the braking manoeuvre are comparable for both PD and INDI controllers (as they increase with time). However, the INDI shows a much faster convergence of rigid body motion (within 250 s) compared to the PD controller (about 600 s). An interesting observation that can be made from Figs. 9(e) and 9(f) is that the control moments after achieving sufficient convergence in rigid body motion, start correcting for the flexible perturbations. This results in a bang-bang control, which ends up exciting the eigenmodes even further. Therefore, for control of flexible perturbations, the selected controllers are insufficient. The performance can be improved by adding active damping to the system. One common way of achieving this, is by introducing bending filters meant for controlling flexible modes. Without any compensatory filter, similar behaviour was observed (Fig. 9), *i.e.*, a strong coupling between rigid body dynamics, flexible modes, and control actions. As stated in Ref. 9, application of modern control methods for flexible structures often result in a feedback loop that is sensitive to the elastic vibrations. Therefore, it is now confirmed that the inclusion of a bending filter can be an important design choice in this research.

B. With Notch Filter

To analyse the effect of notch filter on the signal and to effectively tune it, a second-order filter with a cut-off frequency centred at 0.055 Hz (the main perturbing frequency) is applied in two ways. First, the entire signal is passed through the filter. The filtering process is treated as a post-processing feature and the resultant response is studied. Figures 10(a) and 10(b) show the comparison between the original response obtained from set-point control using INDI and the response after the complete signal is passed through the filter. It can be observed that the response becomes much smoother and the amplitude of vibrations has reduced. However, a filter can behave very differently when it is within a control loop. This can already be observed from the second set of results in which the notch filter is included in the loop. The current state that goes to the controller is passed through the filter, which attempts to smoothen the control input. From Figures 10(c) and 10(d), it can be seen that the filter did not improve the response of the system but instead has lead to huge deviations from the commanded state of $\boldsymbol{\Theta} = (50^\circ, -30^\circ, 60^\circ)^T$. This is because, the target frequency for the filter in this case is very low (0.055Hz). For a second order filter in the control loop, only a small fraction of the sample is passed through. And the lower the order of a filter, the smaller is the delay block. Since the dynamic response of the system changes with every passing loop under the control action, such a filter proves to be ineffective.

For such a low frequency, a higher order filter can accumulate more samples with a larger delay. This allows the filter to gain more experience and recognise the signal characteristics better, thereby resulting in a better response. However, the larger the order of the filter, the larger is the computational effort. Figure 11 shows the response of the flexible multibody control for detumbling and reorientation (full state control) using PD control and a 6th order filter. From the figures, it can be concluded that the higher order filter recognises the system characteristics better and shows much improvement over the second order filter shown in Fig. 10(c). However, in Fig. 11(a) large low frequency oscillations can be observed but the original 0.055 Hz frequency has vanished. This may be because there was an unidentified frequency that was not evidently visible in the original response or was excited because of different control loads. The notch filter was only tuned to remove the 0.055 Hz frequency. This problem can be solved by using two notch filters in a row, to also account for the second frequency. Moreover, a typical filter in a control loop demands that the whole control system is retuned (and not just the filter) to meet the required performance levels. Too aggressive tuning can lead to cycling and overshoots, which would deviate the response further away from the command. It is relatively difficult to tune a multibody control system with a filter in the loop due to the computational effort and gain tuning from a rigid body model is not sufficient. Hence, using a simple filter to directly filter the data is not enough for the current application. Especially because of the low frequency vibrations, a more sophisticated approach is required to find a computationally efficient and easy-to-tune solution for the flexible multibody system.

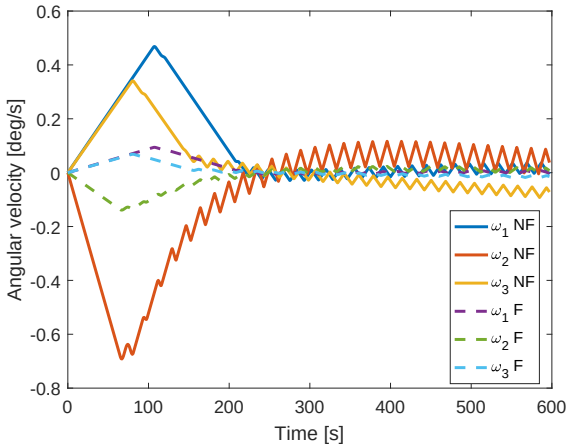

(a) INDI Angular rates - post processing

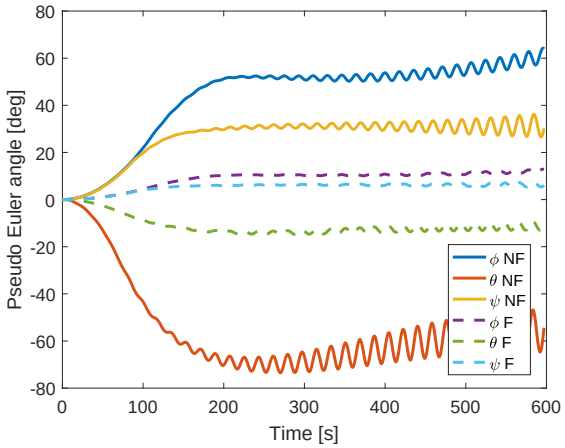

(b) INDI pseudo Euler angles: post processing

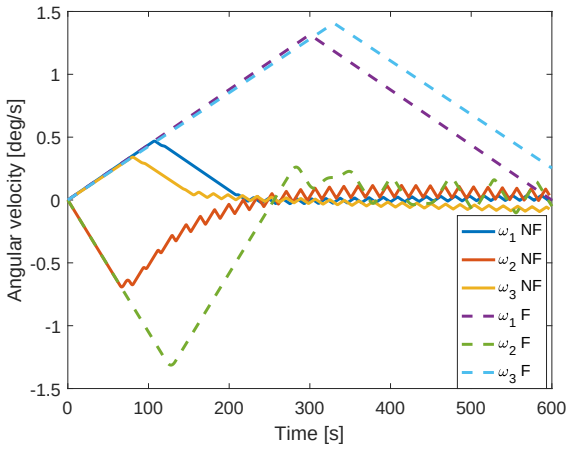

(c) INDI Angular rates: In-loop

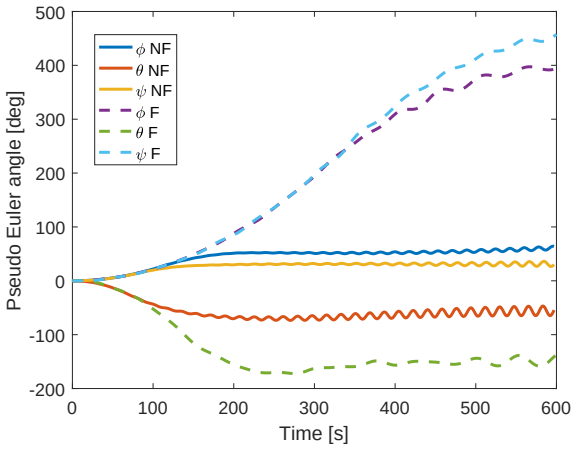

(d) INDI pseudo Euler angles: In-loop

Figure 10. Effect of notch filter on post processed data and In-loop with INDI controller

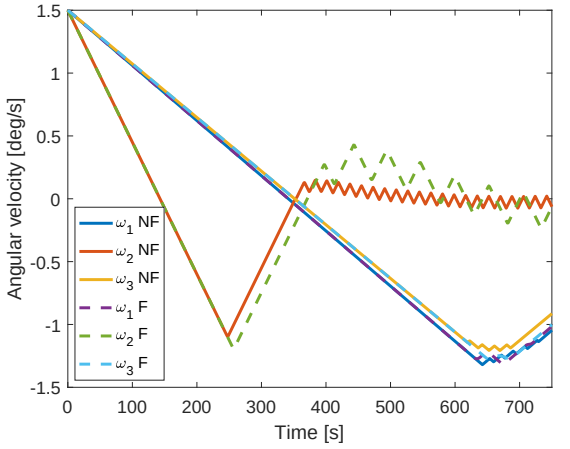

(a) Angular rates

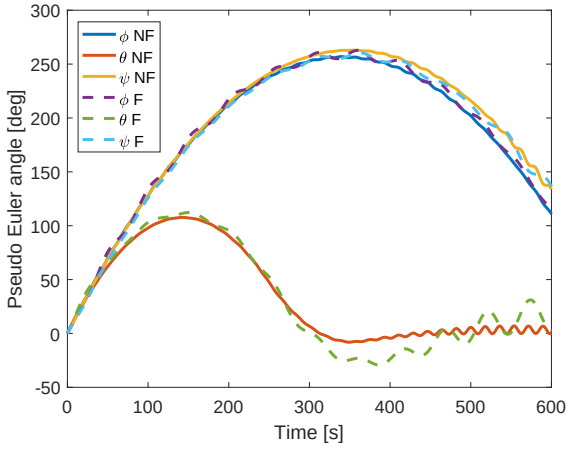

(b) Pseudo Euler Angles

Figure 11. Flexible multibody control (with 6th order notch filter)- Detumbling + Reorientation PD control

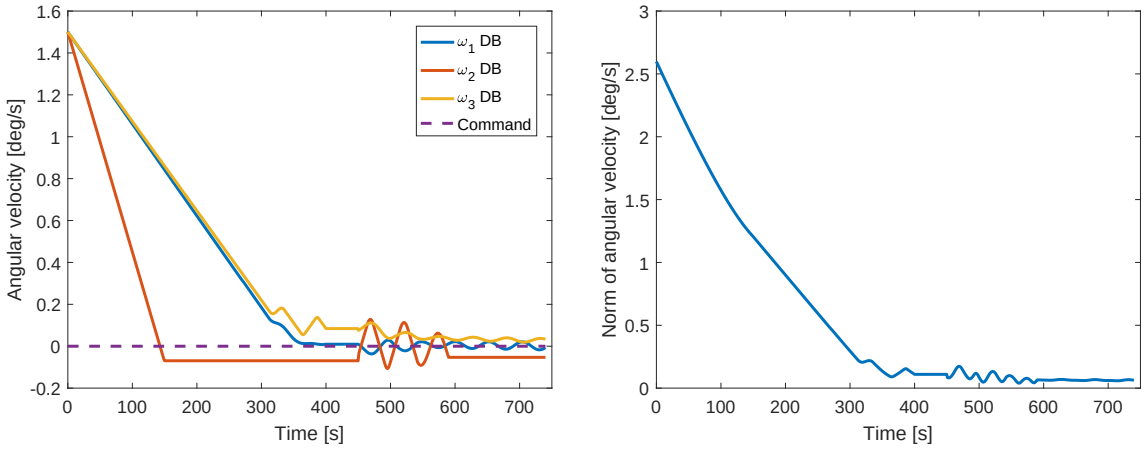

(a) Angular rates

(b) Norm of angular rates

Figure 12. Flexible multibody control (with deadband and damping)- Rate control

C. With Dead-band Control

In this control strategy, a dead-band or zero-control moment band was introduced once sufficient convergence was achieved in the rigid body attitude. Figure 12(a) shows the response of the multibody system for angular rate control from 1.5°/s to 0°/s. It can be observed that during the zero control moment zone (from 150-450 s in X-axis, and 300-450 s in Y- and Z-axis), the oscillations are completely damped out by the passive structural damping. At 450 s, when the control is restarted with lower gains, the response has vibrations with smoother peaks, which seem to be damping out with time. Figure 12(b) confirms the improvement in response as the norm of angular velocity can be seen smoothing out as it approaches zero. Further, this allows the controller to obtain substantial convergence with high gains and then, switch to low gains without aggravating the vibrations. Therefore, this control strategy is an easy yet effective solution for robust control of large flexible structures.

VI. Conclusions and Recommendations

This research continues the work discussed in Ref. 2 and investigates the dynamics and controllability characteristics associated with a chaser spacecraft before, and after docking with a large flexible uncooperative space debris. To improve the controllability, different design approaches were explored. The connected phase was simulated again with the attitude case of 1.5°/s about all axes. A structural damping of 2% for Envisat panel and control limit of ±(10, 5, 10) Nm was used. The results showed considerable improvement over the previously simulated case, and the observed vibrations were reduced to 0.1°/s. Even though the vibrations could not be damped out completely, it was concluded that any errors caused during the deorbitation manoeuvre by such small vibrations, can be corrected by the closed loop guidance system within a finite time. It was again observed that the INDI controller showed faster convergence in the presence of flexible perturbations. Further, after sufficient convergence was achieved in the rigid body motion, the controller attempted to correct the flexible perturbations. This resulted in bang-bang control, which excited the primary eigenfrequency instead of correcting the motion. Therefore, it was concluded that a simple rigid body controller could not be used to control the flexible modes in the system and dedicated bending filters would be required for such corrections. For this purpose, a notch filter was selected to mitigate the dominating frequency of 0.055 Hz. However, a high order filter was required to capture the vibration characteristics of the flexible system, which proved to be computationally heavy. Further, without retuning of the control system with the filter included in the loop, satisfactory results could not be achieved. Tuning the controller with the flexible plant proved to be computationally too demanding to be implemented and thus, the notch filter could not improve the system performance. Finally, a control strategy to reduce the effects of structure-control interactions was tested. In this approach, a zero control moment band (dead-band) was introduced after sufficient rigid body convergence was achieved in the response. This allowed the initial

vibrations to be damped out before the controller is turned out again with lower gains. The approach improved the performance of the system without increasing the computational load and allowed faster control.

For future research, the mission profile of ADR using a chaser satellite can be completed by modelling the semi-connected phase of the mission. In this phase, the chaser and target are connected with one or more flexible links (tentacles), while the complete system is tumbling. It is possible to model the phase as a multibody system with alternating flexible and rigid bodies in a chain like configuration consisting of Envisat panel (flexible) - Envisat hub (rigid) - flexible connection (flexible) - chaser hub (rigid) - chaser panel (flexible). Further, the effect of environmental torques like gravity gradient, atmospheric drag, *etc.*, can also be taken into account. The model can be extended with inclusion of the orbital (translation) motion of the system. This would require the change of attitude representation to Modified Rodrigues Parameters, as pseudo Euler angles will not be practical in this case. In this research, it was assumed that the solar panel rotates at the same rate as the rigid body and only bending modes were analysed. Therefore, the effect of torsional modes of vibrations can also be considered in future work. The structural model of the solar panel can also be improved by modelling it as a plate instead of a beam. From the controls point of view, other types of modern controller can be studied (for instance, simple adaptive control). Also, the effect of non-ideal sensors and actuators can be taken into account. Possible ways of optimising the use of filters (for instance, adaptive tuning) can be studied, and more control strategies can be explored. Lastly, the simulation time can be optimised.

References

[1]Ellenbroek, M.H.M. and Schilder, J., "On the use of absolute interface coordinates in the floating frame of reference formulation for flexible multibody dynamics", *Multibody system dynamics*, Springer 2017.

[2]Singh, S., Mooij, E., and Gransden, D. I., "Multibody Approach to the Controlled Removal of Large Space Debris with Flexible Appendages", AIAA Scitech 2019 Forum.

[3]Schilder, J.P., Ellenbroek, M.H.M. and de Boer, A., "Superelements in a minimal coordinates floating frame of reference formulation.", IMSD, Lisbon, Portugal, 2018.

[4]Craig, R.R., and Bampton, M.C.C., "Coupling of substructures for dynamic analysis", *AIAA Journal*, 6(7), 1313-1319, 1968.

[5]Dwarshuis, K.S., "Geometric Stiffness Formulation for a Superelement", MSc. Thesis, University of Twente, 2017.

[6]Shabana, A.A., "Flexible multibody dynamics: review of past and recent developments", *Multibody system dynamics*, 1(2), pp.189-222., 1997.

[7]Sieberling, S., Chu, Q.P. and Mulder, J.A., "Robust flight control using incremental nonlinear dynamic inversion and angular acceleration prediction", Journal of guidance, control, and dynamics, 33(6), pp.1732-1742, 2010.

[8]Brown, P.N., Byrne, G.D. and Hindmarsh, A.C., "VODE: A Variable Coefficient ODE Solver," *SIAM J. Sci. Stat. Comput.*, Vol. 10, 1989, pp. 1038-1051.

[9]Murphy, C. H., and Mermagen Sr, W. H., "Flight Mechanics of an Elastic Symmetric Missile", *Journal of Guidance, Control and Dynamics*, vol. 24, no. 6., pp. 1125-1132, 2001.

[10]Santini, P., Ottens, H. H., Mead, D. J., Baldacci, R. F., Phillips, E. J., Degener, M., and Wada, B. K. , "Damping Effects in Aerospace Structures", (No. AGARD-CP-277). Advisory Group For Aerospace Research And Development Neuilly-Sur-Seine, France, 1979.

[11]Fujimori, Y., Kato, J., Motohashi, S., Kuwao, F., and Sekimoto, S., "Modal damping measurement of MOS-1 Solar Array Paddle", *Automatic Control in Space* (pp. 121-125), 1985.

[12]Rutkovsky, V. J., Sukhanov, V. M., and Dodds, S. J. , "Definition and dynamic portrait of large space structures for control system synthesis" *WIT Transactions on The Built Environment*, 22, 1970

[13]Gradin, M., and Rixen, D. J., "Mechanical vibrations: theory and application to structural dynamics", John Wiley and Sons, 2014

[14]Tan, L., and Jiang, J., *Digital signal processing: fundamentals and applications*, Academic Press, 2018

[15]Ellis, G.,*Control system design guide: using your computer to understand and diagnose feedback controllers*, Butterworth-Heinemann, 2012

[16]Linskens, H. T. K., and Mooij, E., "Tether dynamics analysis and guidance and control design for active space-debris removal", *Journal of Guidance, Control, and Dynamics*, 1232-1243, 2016

Appendix A. Simulator Architecture

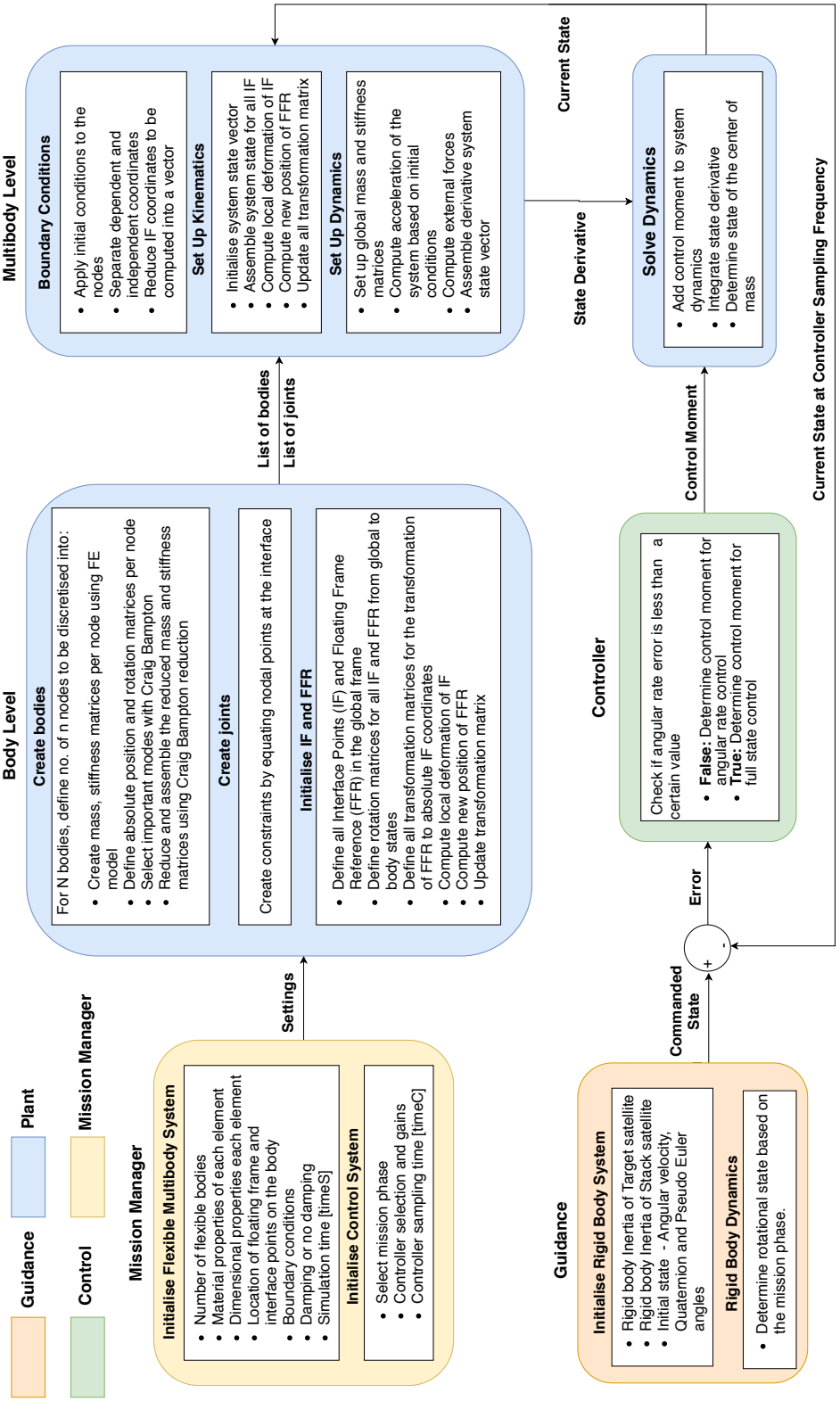

Figure A1. Simulator Architecture